Effects of V and Cu codoping on the tribological properties and oxidation behavior of AlTiN coatings

MEI, Haijuan, DING, Ji Cheng, YAN, Kai, PENG, Weichao, ZHAO, Cancan, LUO, Quanshun <http://orcid.org/0000-0003-4102-2129>, GONG, Weiping, REN, Fuzeng and WANG, Qimin

Accepted on 26 April 2022 for publication in ***Ceramics International***

Effects of V and Cu codoping on the tribological properties and oxidation behavior of AlTiN coatings

Haijuan Mei [a,b,*], Ji Cheng Ding [c], Kai Yan [b], Weichao Peng [a], Cancan Zhao [b], Quanshun Luo [d], Weiping Gong [a], Fuzeng Ren [b,*], Qimin Wang [c,*]

[a] *Guangdong Provincial Key Laboratory of Electronic Functional Materials and Devices, Huizhou University, Huizhou 516007, China*
[b] *Department of Materials Science and Engineering, Southern University of Science and Technology, Shenzhen 518000, China*
[c] *School of Materials Science and Engineering, Anhui University of Technology, Maanshan 243002, China*
[d] *Materials and Engineering Research Institute, Sheffield Hallam University, Sheffield, S1 1 WB, UK*

* Corresponding authors: haijuanmei@hzu.edu.cn (Haijuan Mei), renfz@sustech.edu.cn (Fuzeng Ren), qmwang@gdut.edu.cn (Qimin Wang).

ABSTRACT Due to their high hardness and superior wear resistance, AlTiN coatings have been extensively investigated and used in the field of cutting tools. In this work, the effects of V and Cu codoping on the tribological properties and oxidation behavior of AlTiN coatings were studied. When the Cu content was increased (from 2.6 to 22.6 at.%) and V content decreased (from 16.7 to 2.7 at.%), the wear rates of Al-Ti-V-Cu-N coatings at RT and 300 °C both sharply increased from 10^{-15} to 10^{-14} $m^3/N{\cdot}m$ due to reduced hardness and limited oxidation. At 600 °C, due to outward diffusion and oxidation of Cu, the $Al_{26}Ti_{14}V_3Cu_{22}N_{35}$ coating exhibited the lowest friction coefficient of 0.5 and wear rate of 3.2×10^{-15} $m^3/N{\cdot}m$. The increase of V content reduced the oxidation resistance of the Al-Ti-V-Cu-N coatings, and the oxidation mechanism of the V-rich $Al_{21}Ti_{12}V_{17}Cu_3N_{47}$ coating involved mainly the outward diffusion of elements Al, V, and Cu and the formation of mixed oxides $AlVO_4$, V_2O_5, and CuO on the top layer. Increasing the Cu content promoted the outward diffusion and oxidation of Cu and the formation of a smooth top layer of CuO, contributing to excellent wear performance.

Keywords: AlTiN; V-Cu; Tribological properties; Oxidation behavior.

1. Introduction

In recent years, Ti-Al-V-N coatings have been widely investigated and applied as low-friction and anti-wear coatings [1–5]. Due to the formation of lubricious oxides (e.g., V_2O_5) at high temperatures, TiAlN coatings that are alloyed with V are potential candidates for the self-lubricating coatings [6, 7]. The microstructural evolution and mechanical and tribological properties of Ti-Al-V-N coatings have been thoroughly investigated in other papers [8–10]. At room temperature (RT), due to the decrease of tribo-chemical reactions of Ti and the solid solution hardening effect, the addition of V into TiAlN coatings was observed to not only reduce the friction coefficient but also enhance the wear resistance. At 500 °C, due to reduced oxidation resistance, the wear resistance decreased with increasing V content. At 700 °C, despite a pronounced reduction in friction coefficient, the wear resistance sharply decreased due to severe oxidation. The high-temperature oxidation behavior of TiAlVN coatings was studied by Xu et al. [11], and found that the addition of V into TiAlN coatings resulted in an earlier formation of TiO_2 oxide and reduced the oxidation resistance. Thus, the rapid oxidation of Ti-Al-V-N coatings at elevated temperatures promoted the formation of V-O lubricious oxides, which led to a decrease in the friction coefficient but also caused a loss of mechanical stability and a decrease in wear resistance.

Recently, various soft metals (e.g., Au, Ag and Cu) have been incorporated into hard

coatings to form nanocomposite or multilayer structures (e.g., CrN-Ag [12, 13], Mo-Cu-N [14], and AlTiN/Cu [15]) to provide lubrication properties by the outward diffusion of soft metals. For instance, the addition of Cu into CrN coatings promoted the formation of complex oxides at 150 °C, which enhanced tribological performance [16]. In addition, the outward diffusion of Cu at 400 °C contributed to a decrease in the friction coefficient, and lower friction coefficient values were obtained for higher Cu contents [17]. At low-moderate temperatures, the tribological properties of hard coatings were further improved by the outward diffusion of soft metals [18].

However, few studies have focused on the outward diffusion and oxidation of Cu metal at moderate temperatures, and its relation to the tribological behavior of hard coatings. In previous work [19], it was shown that the addition of Cu significantly affected the micro-structure and mechanical properties of Al-Ti-V-N coatings, but the high-temperature oxidation behavior and tribological properties should be further investigated. Thus, the aim of this study was to investigate the influence of V and Cu codoping on the tribological properties and oxidation behavior of AlTiN coatings.

2. Experimental

Al-Ti-V-Cu-N coatings were prepared on polished substrates of YT14 cemented carbide by high-power impulse magnetron sputtering (HIPIMS) with a $Al_{67}Ti_{33}$-V-Cu target (99.9% purity), which consisted of a $Al_{67}Ti_{33}$ alloy target and V-Cu metal target. Before deposition, all the samples were ultrasonically cleaned in pure acetone and alcohol. To enhance the adhesion strength, a thin CrN layer (~ 100 nm) was deposited by arc ion plating for 5 min in a pure nitrogen atmosphere. Then, the Al-Ti-V-Cu-N coatings were prepared by HIPIMS in a mixed atmosphere of Ar and N_2 at a total gas pressure of 0.6 Pa. The target power was set at 1.5 kW with a duty cycle of 2%, additional details regarding the deposition parameter were reported in a previous study [19]. Three vertical substrate distances (D = 4, 10, and 16 cm) were used to prepare the coatings with various chemical compositions, which corresponded to the $Al_{21}Ti_{12}V_{17}Cu_3N_{47}$, $Al_{26}Ti_{14}V_9Cu_8N_{43}$, and $Al_{26}Ti_{14}V_3Cu_{22}N_{35}$ coatings, as listed in Table 1. The coating thickness reached 0.8 ~ 1.6 μm after deposition for 180 min.

Table 1 Chemical compositions and mechanical properties of the Al-Ti-V-Cu-N coatings [19].

Coating	Chemical composition (at.%)					Thickness (μm)	Hardness (GPa)
	Al	Ti	V	Cu	N		
$Al_{21}Ti_{12}V_{17}Cu_3N_{47}$	21.0	12.6	16.7	2.6	47.1	0.8	41.1 ± 1.0
$Al_{26}Ti_{14}V_9Cu_8N_{43}$	26.3	13.8	8.6	8.3	43.0	1.1	34.5 ± 0.9
$Al_{26}Ti_{14}V_3Cu_{22}N_{35}$	26.2	13.7	2.7	22.6	34.8	1.6	14.9 ± 0.6

The tribological properties were tested by using a ball-on-disc tribometer (THT, CSM, Switzerland) at room temperature (RT), 300 °C, 600 °C in ambient atmosphere. All wear tests were carried out for 5000 cycles at a normal load of 2 N. After the wear tests, a confocal laser scanning microscope (OLS4100, Olympus, Japan) was used to characterize wear scar profiles. The oxidized and worn surfaces were characterized by scanning electron microscopy (SEM, Quanta 650, Czech Republic) that was equipped with a spectrometer for energy-dispersive X-ray spectrometry (EDS). The oxidized phases were characterized by X-ray diffraction (XRD, D8 Advance, Germany) with Cu K_α radiation. The tribo-oxides formed on worn surfaces were analyzed by X-ray photoelectron spectroscopy

(XPS, Escalab 250Xi, USA) with Al K_α irradiation.

3. Results and discussion

3.1. Tribological properties

In Table 1, based on stoichiometric ratios, the AlTiN-V(16.7 at.%)-Cu(2.6 at.%), AlTiN-V(8.6 at.%)-Cu(8.3 at.%), and AlTiN-V(2.7 at.%)-Cu(22.6 at.%) contents corresponded to $Al_{21}Ti_{12}V_{17}Cu_3N_{47}$, $Al_{26}Ti_{14}V_9Cu_8N_{43}$, and $Al_{26}Ti_{14}V_3Cu_{22}N_{35}$ coatings, respectively. Fig. 1 displays the friction coefficients of Al-Ti-V-Cu-N coatings at RT, 300 °C, and 600 °C. The $Al_{21}Ti_{12}V_{17}Cu_3N_{47}$ and $Al_{26}Ti_{14}V_9Cu_8N_{43}$ coatings exhibited similar tendencies over all temperature ranges from RT to 600 °C. At RT, a slight increase from 0.66 to 0.88 was observed in the average friction coefficient when the Cu content increased. At 300 °C, the water vapor vanished from the test environment, and the hydrated tribofilm that formed at RT disappeared [20], thereby leading to sharp increases in the friction coefficient to 0.99 and 1.04 for the $Al_{21}Ti_{12}V_{17}Cu_3N_{47}$ and $Al_{26}Ti_{14}V_9Cu_8N_{43}$ coatings, respectively. Similar phenomenon was also observed for the Mo-V-Cu-N coatings, namely, the friction coefficient sharply increased at 300 °C [17]. However, the average friction coefficient of the $Al_{26}Ti_{14}V_3Cu_{22}N_{35}$ coating sharply decreased to 0.49 at 300 °C, which could be due to the outward diffusion of Cu and will be discussed later. At 600 °C, the friction coefficient decreased slightly to 0.66 and 0.90 for the $Al_{21}Ti_{12}V_{17}Cu_3N_{47}$ and $Al_{26}Ti_{14}V_9Cu_8N_{43}$ coatings, respectively. The lowest friction coefficient of 0.50 was achieved for the $Al_{26}Ti_{14}V_3Cu_{22}N_{35}$ coating, which was related to the outward diffusion and oxidation of Cu.

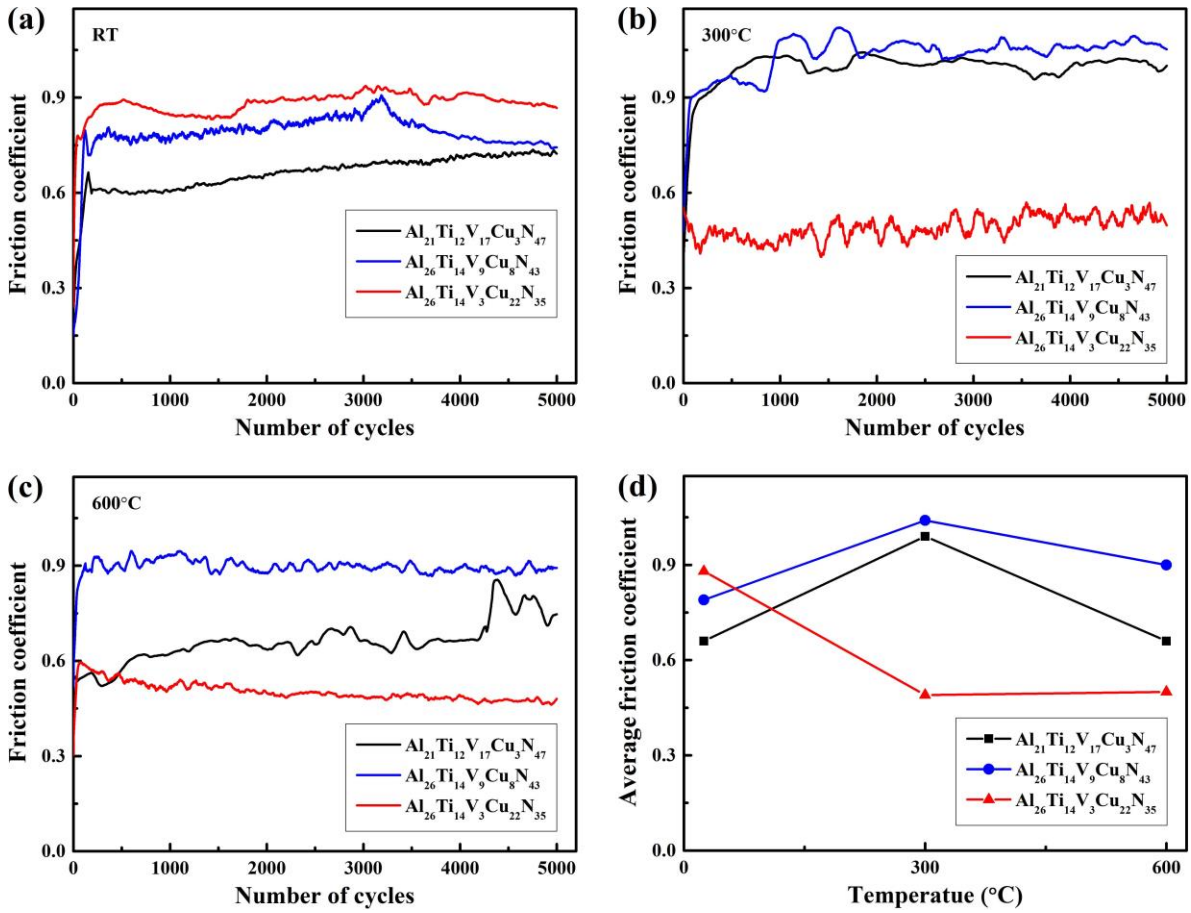

Fig. 1. Friction coefficients of Al-Ti-V-Cu-N coatings at various temperatures: (a) RT, (b) 300 °C, (c) 600 °C, and (d) average friction coefficient.

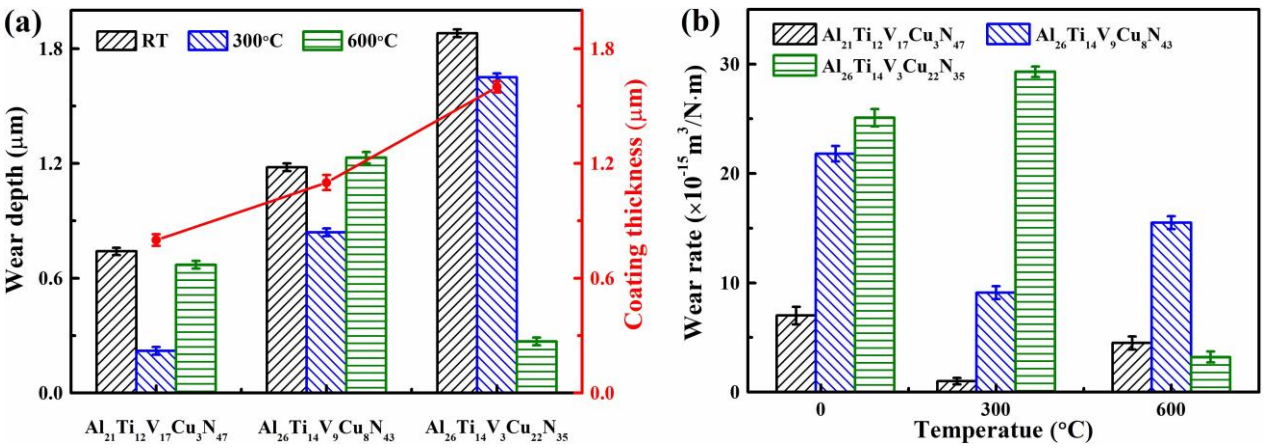

Fig. 2. Wear depths and coating thicknesses (a) and wear rates (b) of the coatings at various temperatures.

Fig. 2(a) displays the wear depths and coating thicknesses at various temperatures. For the $Al_{21}Ti_{12}V_{17}Cu_3N_{47}$ coating, all the wear depths were lower than the coating thicknesses, indicating that the coating exhibited excellent wear resistance over a wide temperature range. However, for the $Al_{26}Ti_{14}V_9Cu_8N_{43}$ coating, at RT and 600 °C, the wear depths were higher than the coating thicknesses, indicating that the coating had been completely worn out. Similar results were also found for the $Al_{26}Ti_{14}V_3Cu_{22}N_{35}$ coating at RT and 300 °C, which indicated the coating had been completely worn out. However, the wear depth sharply decreased to 0.27 μm at 600 °C, thereby implying an increase in wear resistance. Fig. 2(b) presents the wear rates of Al-Ti-V-Cu-N coatings, which exhibited a similar tendency to the wear depth. With increasing Cu content, the wear rate sharply increased from 7.0×10^{-15} to 2.5×10^{-14} $m^3/N \cdot m$ at RT and from 1.0×10^{-15} to 2.9×10^{-14} $m^3/N \cdot m$ at 300 °C. The decrease in wear resistance could have been due to the limited oxidation of the coatings and reduced hardness at higher Cu contents (in Table 1). However, at 600 °C, with increasing Cu content, the wear rate initially increased from 4.5×10^{-15} to 1.6×10^{-14} $m^3/N \cdot m$ and subsequently decreased to 3.2×10^{-15} $m^3/N \cdot m$, indicating that the $Al_{26}Ti_{14}V_3Cu_{22}N_{35}$ coating exhibited the best wear resistance, which can be related to the following tribo-oxidation behavior.

3.2. Oxidation behavior

Fig. 3 shows the XRD patterns of the Al-Ti-V-Cu-N coatings after the wear tests. All the coatings showed a Ti-Al-V-N solid-solution phase, and no obvious changes in the phase structure were observed at 300 °C. In Fig. 3(a), for the $Al_{21}Ti_{12}V_{17}Cu_3N_{47}$ coating, the diffraction intensity of nitride was significantly reduced at 600 °C. In addition, many oxide peaks, including those of V_2O_5, $AlVO_4$, and minor oxides such as CuO, were detected in the XRD pattern, implying that severe oxidation occurred at 600 °C. Among these oxides, $AlVO_4$ was mainly formed by the solid-state reaction between V_2O_5 and Al_2O_3 [21]. As shown in Fig. 3(b), for the $Al_{26}Ti_{14}V_9Cu_8N_{43}$ coating, no oxide phases were detected by XRD, indicating that the decrease in V content contributed to an improvement in the oxidation resistance. When the temperature was increased, the diffraction peaks of nitride shifted toward higher diffraction angles, implying the relaxation of residual stress, which could be caused by the annihilation and/or arrangement of microstructure defects in the coatings [11]. In Fig. 3(c), for the $Al_{26}Ti_{14}V_3Cu_{22}N_{35}$ coating, it was found that CuO appeared at 600 °C, implying that higher Cu content promoted the outward diffusion and oxidation of Cu.

The surface micrographs of the Al-Ti-V-Cu-N coatings after wear at RT and 300 °C are compared in Fig. 4. At RT, all the coating surfaces were uniformly covered with

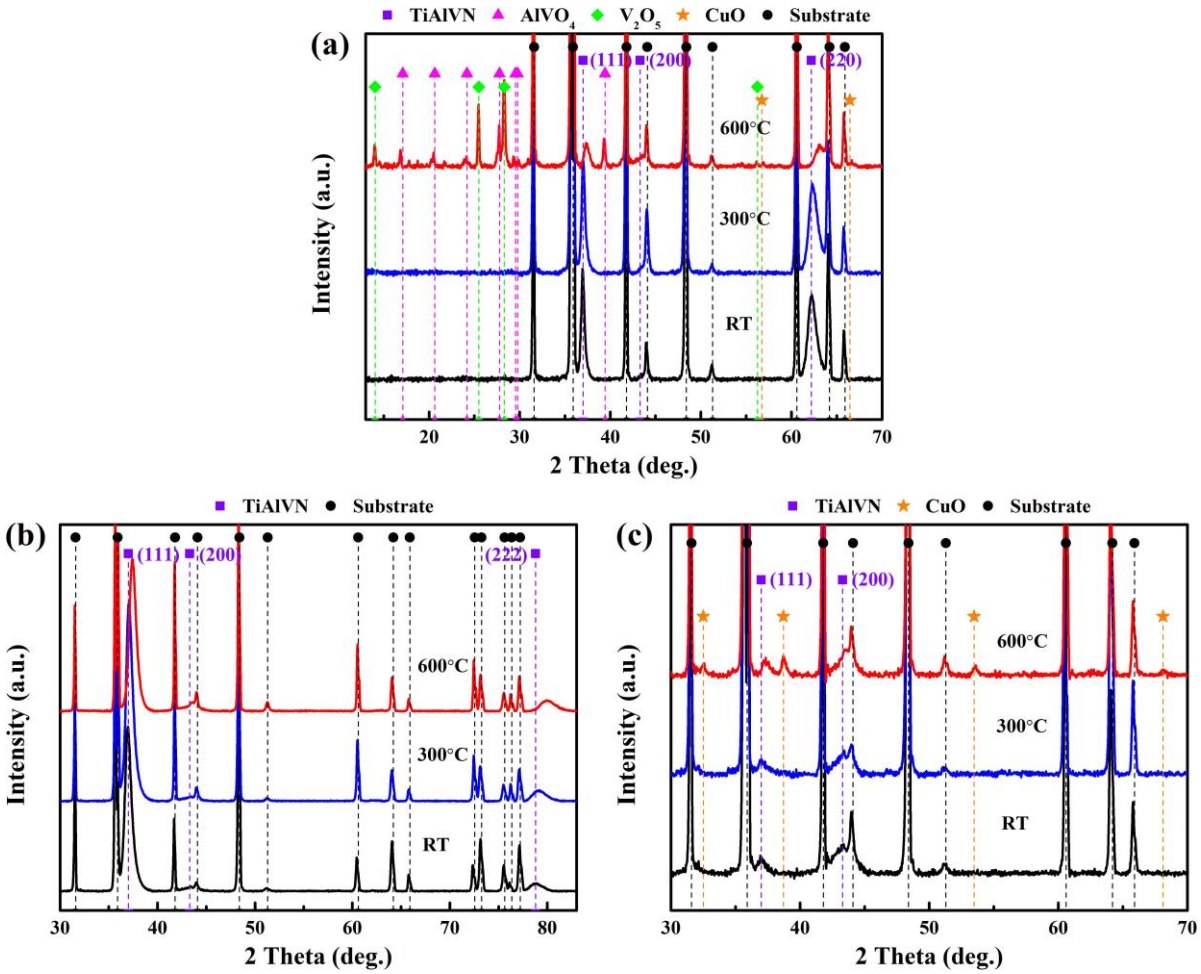

Fig. 3. XRD patterns of Al-Ti-V-Cu-N coatings after wear at various temperatures: (a) $Al_{21}Ti_{12}V_{17}Cu_3N_{47}$, (b) $Al_{26}Ti_{14}V_9Cu_8N_{43}$, and (c) $Al_{26}Ti_{14}V_3Cu_{22}N_{35}$.

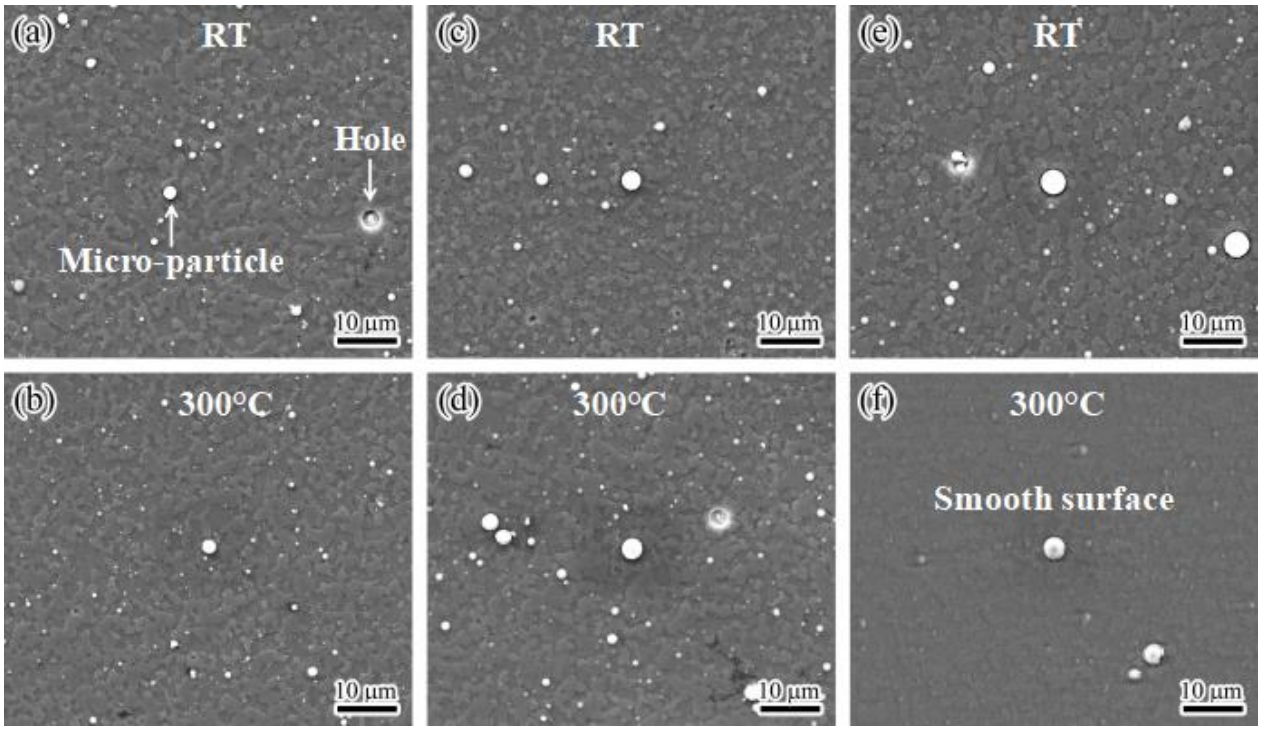

Fig. 4. Surface SEM images of Al-Ti-V-Cu-N coatings after wear at RT and 300 °C: (a, b) $Al_{21}Ti_{12}V_{17}Cu_3N_{47}$, (c, d) $Al_{26}Ti_{14}V_9Cu_8N_{43}$, and (e, f) $Al_{26}Ti_{14}V_3Cu_{22}N_{35}$.

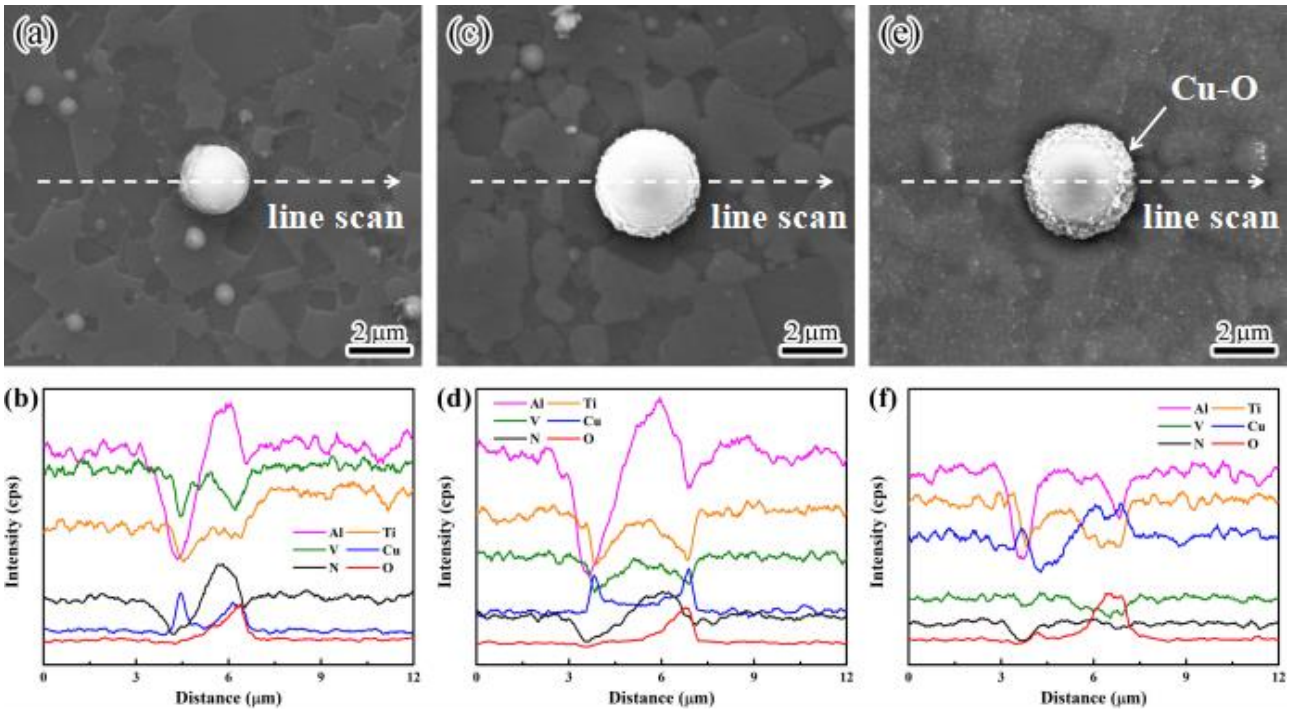

Fig. 5. Oxidized surfaces and EDS line scans of Al-Ti-V-Cu-N coatings after wear at 300 °C: (a, b) $Al_{21}Ti_{12}V_{17}Cu_3N_{47}$, (c, d) $Al_{26}Ti_{14}V_9Cu_8N_{43}$, (e, f) $Al_{26}Ti_{14}V_3Cu_{22}N_{35}$.

Table 2 Chemical compositions of the oxidized surfaces at various temperatures according to EDS analysis, error ± 0.5 at.%.

Temperature	Coating	Chemical composition (at.%)					
		Al	Ti	V	Cu	N	O
RT	$Al_{21}Ti_{12}V_{17}Cu_3N_{47}$	20.2	12.3	16.2	2.4	42.5	6.4
	$Al_{26}Ti_{14}V_9Cu_8N_{43}$	26.7	13.8	8.3	7.7	38.4	5.1
	$Al_{26}Ti_{14}V_3Cu_{22}N_{35}$	26.4	13.4	2.8	22.0	31.7	3.7
300 °C	$Al_{21}Ti_{12}V_{17}Cu_3N_{47}$	19.5	11.2	15.0	2.6	45.1	6.6
	$Al_{26}Ti_{14}V_9Cu_8N_{43}$	25.2	13.0	8.2	7.3	38.7	7.6
	$Al_{26}Ti_{14}V_3Cu_{22}N_{35}$	26.1	13.5	2.7	22.0	26.8	8.9
600 °C	$Al_{21}Ti_{12}V_{17}Cu_3N_{47}$	18.0	10.6	15.4	2.5	–	53.5
	$Al_{26}Ti_{14}V_9Cu_8N_{43}$	23.4	12.4	7.7	6.8	33.2	16.5
	$Al_{26}Ti_{14}V_3Cu_{22}N_{35}$	15.8	10.2	2.1	17.6	–	54.3

microparticles and holes, which was caused by high ion bombardment and arcing events during coating deposition [22]. At 300 °C, no obvious changes were observed in the coatings in Fig. 4(b, d). However, the coating surface became much smoother in Fig. 4(f), and the O content of the coating surface increased to 8.9 at.% (in Table 2). This implied that the $Al_{26}Ti_{14}V_3Cu_{22}N_{35}$ coating had been slightly oxidized, and the formed smooth surface contributed to a decrease in the friction coefficient. To further analyze the slight oxidation at 300 °C, magnified images of the oxidized surfaces are compared in Fig. 5. In Fig. 5(e), many small oxide particles were distributed around the edge of the microparticle, which corresponded to the Cu-O based on the EDS line scan in Fig. 5(f). It can be inferred that at a high Cu content of 22.6 at.%, outward diffusion of Cu occurred at 300 °C, which preferentially diffused through the voids around growth defects and led to a decrease in the friction coefficient [17].

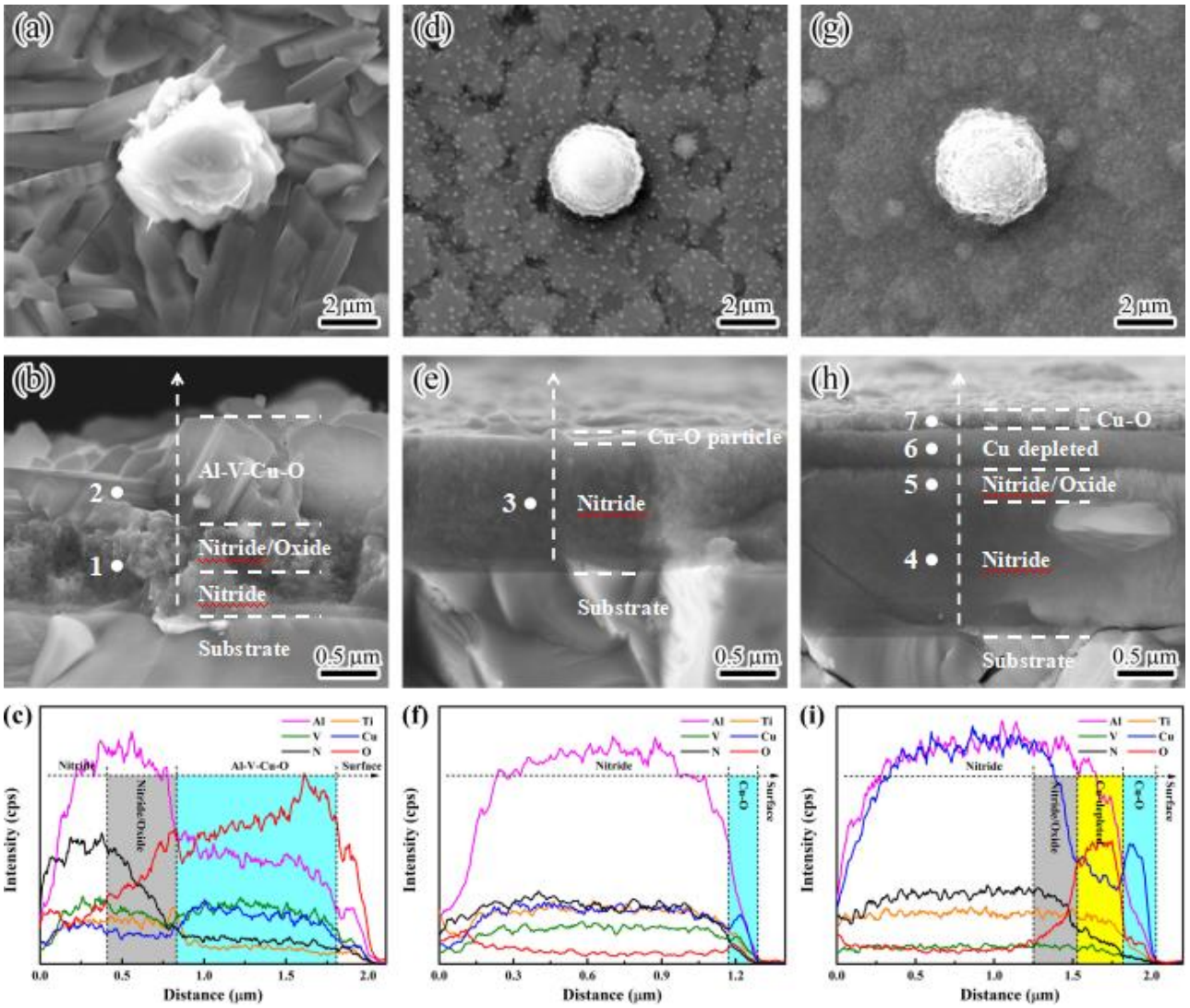

Fig. 6. Oxidized surfaces, cross-sections and EDS line scans of the coatings after wear at 600 °C: (a–c) $Al_{21}Ti_{12}V_{17}Cu_3N_{47}$, (d–f) $Al_{26}Ti_{14}V_9Cu_8N_{43}$, (g–i) $Al_{26}Ti_{14}V_3Cu_{22}N_{35}$. The white dots refer to the selected areas that were analyzed by EDS in Table 3.

The oxidized surfaces and cross-sections of the Al-Ti-V-Cu-N coatings at 600 °C are shown in Fig. 6. For the $Al_{21}Ti_{12}V_{17}Cu_3N_{47}$ coating in Fig. 6(a–c), numerous rod-shaped oxides appeared on the coating surface, indicating that the coating surface was completely oxidized. Based on the EDS line scan, the cross-section coating was divided into three layers, namely, a nitride coating layer, nitride/oxide coating layer, and oxide layer. The top layer, which had a thickness of ~ 1.0 μm, corresponded to the rod-shaped oxides that were observed on the coating surface. The EDS results of area 2 (in Table 3) revealed that these oxides were rich in elements Al, V, and Cu, which was consistent with the EDS line scan. Based on the XRD results in Fig. 6(a), these oxides were identified as $AlVO_4$, V_2O_5, and CuO. Thus, it can be inferred that the oxidation mechanism of the V-rich $Al_{21}Ti_{12}V_{17}Cu_3N_{47}$ coating involved mainly the outward diffusion of elements Al, V, and Cu to the oxide/vapor interface and the simultaneous inward diffusion of O to the oxide/nitride interface.

As presented in Fig. 6(b) and Table 3, along the direction of outward diffusion, the V/Al ratio sharply increased from 0.65 (in area 1) to 1.39 (in area 2), thereby suggesting that the outward diffusion of V was faster than that of Al, which was consistent with above XRD result that the oxides were dominated by V_2O_5. Similar oxidation behavior was also observed in the TiAlN/VN coatings, and V exhibited the fastest diffusion rate due to the formation of V-O outer oxides [23]. However, no Al_2O_3 oxide phase was identified in above

XRD results. This was due to the formed $AlVO_4$ disrupting the formation of an Al_2O_3 protective layer on the coating surfaces [21], which led to the rapid oxidation of the $Al_{21}Ti_{12}V_{17}Cu_3N_{47}$ coating at 600 °C. In addition, the formation of $AlVO_4$ was also responsible for an increase in the friction coefficient [10] to a high value of 0.66 despite the formation of V_2O_5 lubricious oxide.

Table 3 Chemical compositions of the cross-sections at 600 °C according to EDS analysis, error ± 0.5 at.%.

Coating	Area	Chemical composition (at.%)					
		Al	Ti	V	Cu	N	O
$Al_{21}Ti_{12}V_{17}Cu_3N_{47}$	1	15.9	6.9	10.3	2.1	36.2	28.6
	2	12.2	3.6	17.0	5.2	−	62.0
$Al_{26}Ti_{14}V_9Cu_8N_{43}$	3	27.0	14.1	8.7	6.9	38.2	5.1
	4	24.6	10.8	1.9	19.9	42.8	−
$Al_{26}Ti_{14}V_3Cu_{22}N_{35}$	5	29.9	14.2	2.6	20.8	20.5	12.0
	6	22.8	12.9	2.3	7.6	−	54.4
	7	4.2	1.5	−	39.5	−	54.8

For the $Al_{26}Ti_{14}V_9Cu_8N_{43}$ coating in Fig. 6(d–f), small particles appeared on the coating surface, and the EDS results showed a low O content of 16.5 at.%, which implied that the coating surface was slightly oxidized. Based on an analysis of the cross-section and EDS line scan results, these small particles on the coating surface corresponded to Cu-O, thereby indicating that outward diffusion of Cu also occurred for the $Al_{26}Ti_{14}V_9Cu_8N_{43}$ coating at 600 °C, which led to a decrease in the friction coefficient, as shown in Fig. 1(d). However, outward diffusion of V was not observed in the cross-section of the coating, and no V-O oxides were identified in the above XRD results. Thus, the outward diffusion of Cu preferentially occurred over that of V even at almost equal contents. In addition, the cross-section coating retained a dense microstructure, and the EDS analysis of area 3 (in Table 3) revealed a relatively low O content of 5.1 at.%, thereby indicating that the $Al_{26}Ti_{14}V_9Cu_8N_{43}$ coating exhibited excellent oxidation resistance at 600 °C.

For the $Al_{26}Ti_{14}V_3Cu_{22}N_{35}$ coating in Fig. 6(g–i), the coating surface became much smoother, and the particles on coating surface were almost completely oxidized. Based on an analysis of the EDS line scan, the cross-section coating was divided into four layers: a nitride coating layer (~ 1.2 μm), nitride/oxide coating layer (~ 0.3 μm), Cu-depleted layer (~ 0.3 μm), and Cu-O layer (~ 0.2 μm). Based on the EDS results of area 6 and area 7 (in Table 3), the Cu-depleted layer was completely oxidized, and the top layer was rich in elements Cu and O, which corresponded to CuO based on the above XRD results. This indicated that the $Al_{26}Ti_{14}V_3Cu_{22}N_{35}$ coatings with high Cu contents provided a sufficient amount of Cu to diffuse outward at 600 °C and formed a thin and smooth layer of CuO on the coating surface, which exhibited an excellent lubrication effect, thereby contributing to a low friction coefficient and excellent wear resistance. Thus, the oxidation mechanism of the Cu-rich $Al_{26}Ti_{14}V_3Cu_{22}N_{35}$ coating involved mainly the outward diffusion of Cu and simultaneous inward diffusion of O. A schematic diagram of the diffusion and oxidation mechanisms of V-rich and Cu-rich Al-Ti-V-Cu-N coatings is shown in Fig. 7.

3.3. Wear mechanism

Fig. 8 presents the worn surfaces and EDS results of the Al-Ti-V-Cu-N coatings at room temperature (RT). In Fig. 8(a, d, g), the wear tracks became much wider and deeper

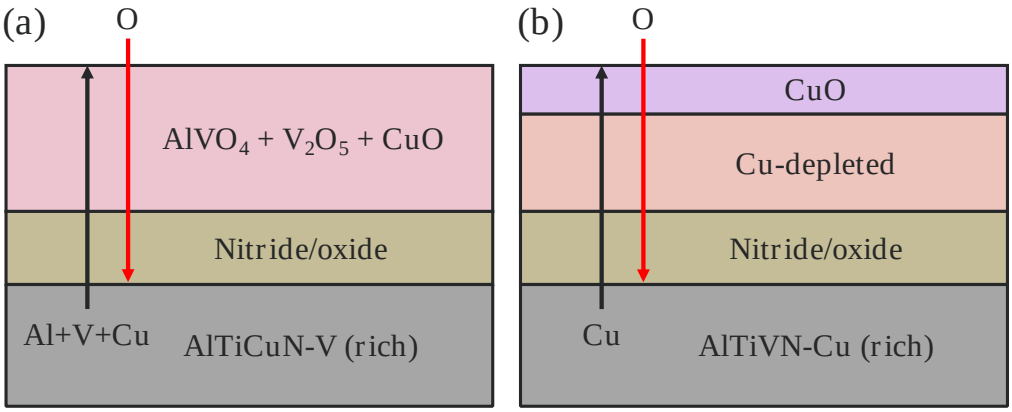

Fig. 7. Schematic diagram of the diffusion and oxidation mechanism of Al-Ti-V-Cu-N coatings: (a) V-rich coatings, and (b) Cu-rich coatings.

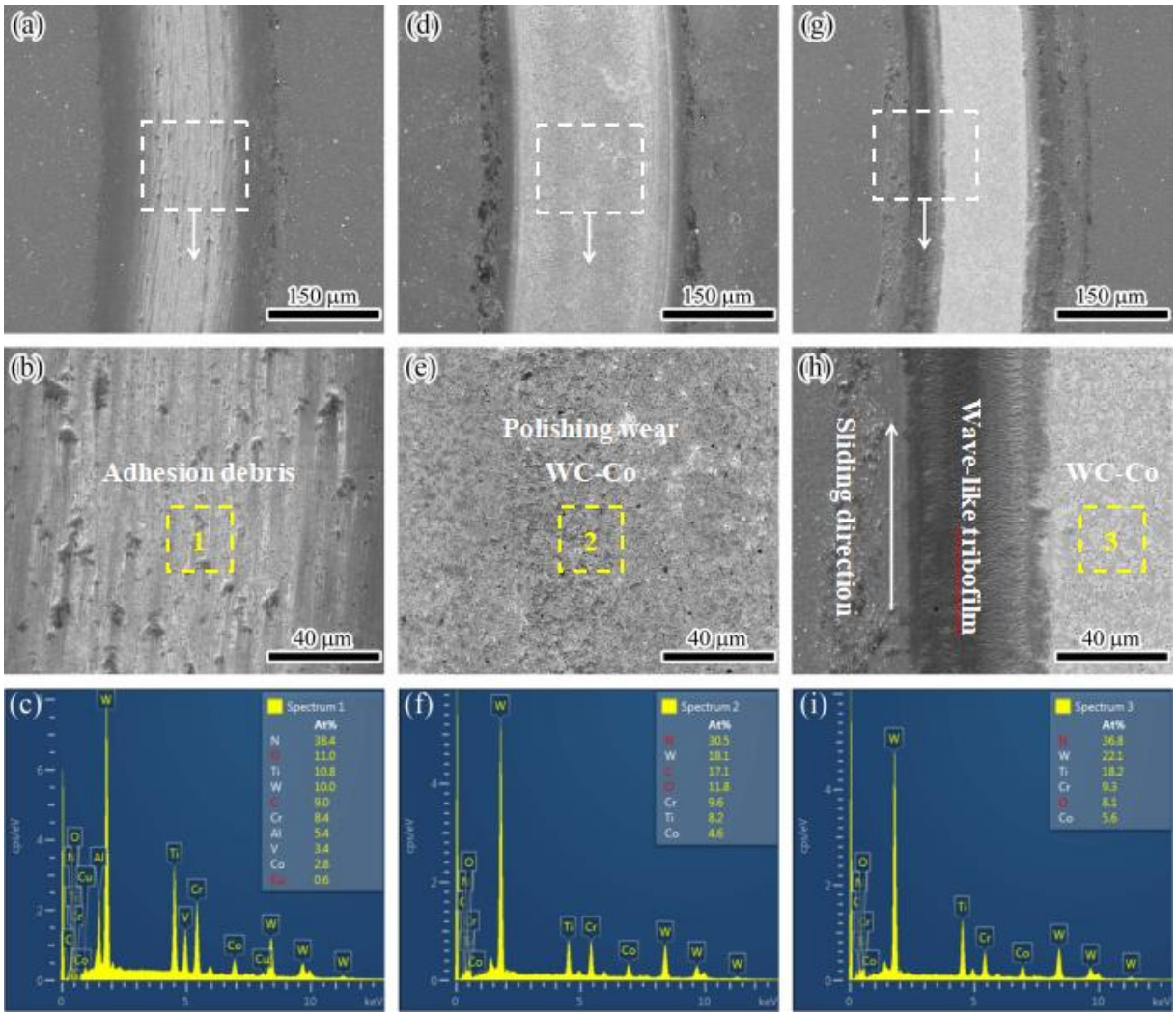

Fig. 8. Worn surfaces, high-magnification images and EDS results of the wear tracks at RT: (a–c) $Al_{21}Ti_{12}V_{17}Cu_3N_{47}$, (d–f) $Al_{26}Ti_{14}V_9Cu_8N_{43}$, (g–i) $Al_{26}Ti_{14}V_3Cu_{22}N_{35}$.

with increasing the Cu content, which increased the friction contact area and adhesive attraction during the sliding process and led to an increase in the friction coefficient. Magnified images of the selected worn surfaces are compared in Fig. 8(b, e, h). As shown in Fig. 8(b), grooves and adhesion debris on the worn surface were observed for the

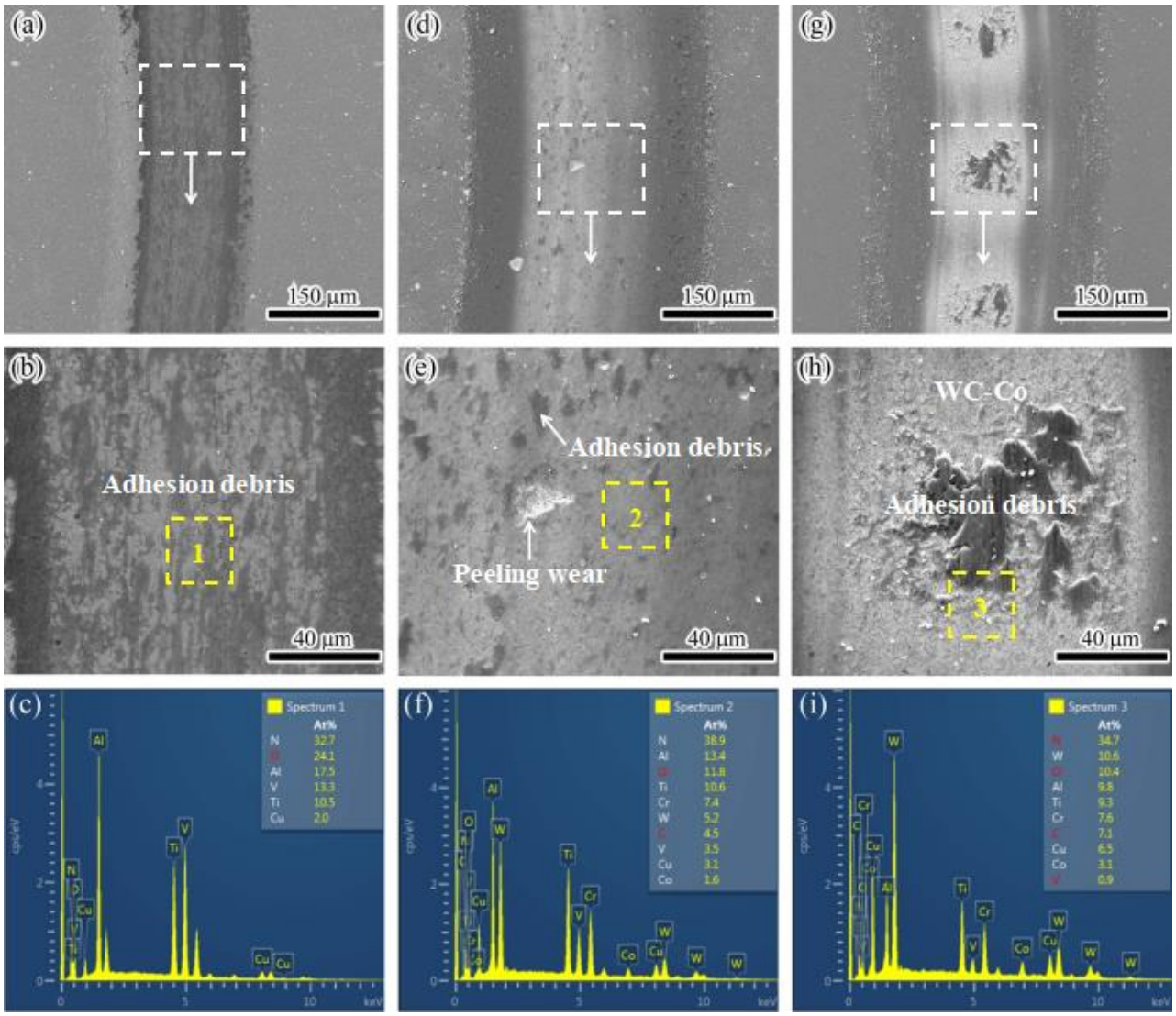

Fig. 9. Worn surfaces, high-magnification images and EDS results of the wear tracks at 300 °C: (a–c) $Al_{21}Ti_{12}V_{17}Cu_3N_{47}$, (d–f) $Al_{26}Ti_{14}V_9Cu_8N_{43}$, (g–i) $Al_{26}Ti_{14}V_3Cu_{22}N_{35}$.

$Al_{21}Ti_{12}V_{17}Cu_3N_{47}$ coating, implying that the wear mechanism was dominated by abrasive and adhesion wear at RT. In Fig. 8(e), the $Al_{26}Ti_{14}V_9Cu_8N_{43}$ coating exhibited a flat worn surface for which the wear was similar to polishing wear. For the $Al_{26}Ti_{14}V_3Cu_{22}N_{35}$ coating in Fig. 8(h), a wave-like tribofilm formed along the sliding direction on the edge of worn surface, and the center area of the worn surface presented a polished surface that was similar to that of the cemented carbide substrate. Based on the EDS results in Fig. 8(f, i), it was found that the worn surfaces were rich in elements W, C, and Co, indicating that the $Al_{26}Ti_{14}V_9Cu_8N_{43}$ and $Al_{26}Ti_{14}V_3Cu_{22}N_{35}$ coatings were completely worn out and that the WC-Co substrate was exposed, which was consistent with the results of the wear depth analysis in Fig. 2(a). Thus, the wear mechanism transformed into mechanical and polishing wear.

The worn surfaces of the Al-Ti-V-Cu-N coatings after the wear tests at 300 °C are presented in Fig. 9. As shown in Fig. 9(a), for the $Al_{21}Ti_{12}V_{17}Cu_3N_{47}$ coating, the wear track was much shallower and narrower than that at RT, indicating an excellent wear resistance at 300 °C. This improvement in wear resistance would be attributed to the absence of humidity [24], the formation of an Al_2O_3 protective layer [25], and the decrease in fracture probability at elevated temperatures [26]. As shown in Fig. 9(b), many adhesion debris can

be clearly observed in the magnified image of worn surface, and the EDS analysis of the worn surface revealed that the O content increased up to 24.1 at.%, indicating that the wear mechanism was dominated by adhesion wear and mild oxidation wear at 300 °C. For the $Al_{26}Ti_{14}V_9Cu_8N_{43}$ coating in Fig. 9(d–f), some microparticles on worn surface were compacted and/or peeled off during the sliding process, which resulted in adhesion and peeling wear. The EDS analysis of the worn surface showed a low O content of 11.8 at.%, which implied that the oxidation wear was limited. Thus, the relatively high friction coefficient at 300 °C in Fig. 1 would be caused by cracking and spalling wear [27]. For the $Al_{26}Ti_{14}V_3Cu_{22}N_{35}$ coating in Fig. 9(g–i), some adhesion debris accumulated on the worn surface, and the polished worn surface was rich in elements W, C, and Co, indicating that the coating was completely worn out and the WC-Co substrate was exposed. Despite the formation of a smooth surface by the outward diffusion of Cu at 300 °C, but the oxidation was limited, and the smooth outer layer was too thin to act as a protective layer, thereby leading to a decrease in wear resistance.

The worn surfaces of the Al-Ti-V-Cu-N coatings after the wear tests at 600 °C are compared in Fig. 10. For the $Al_{21}Ti_{12}V_{17}Cu_3N_{47}$ coating in Fig. 10(a–c), the worn surface was severely oxidized and covered with many leaf-shaped oxides. The EDS analysis of

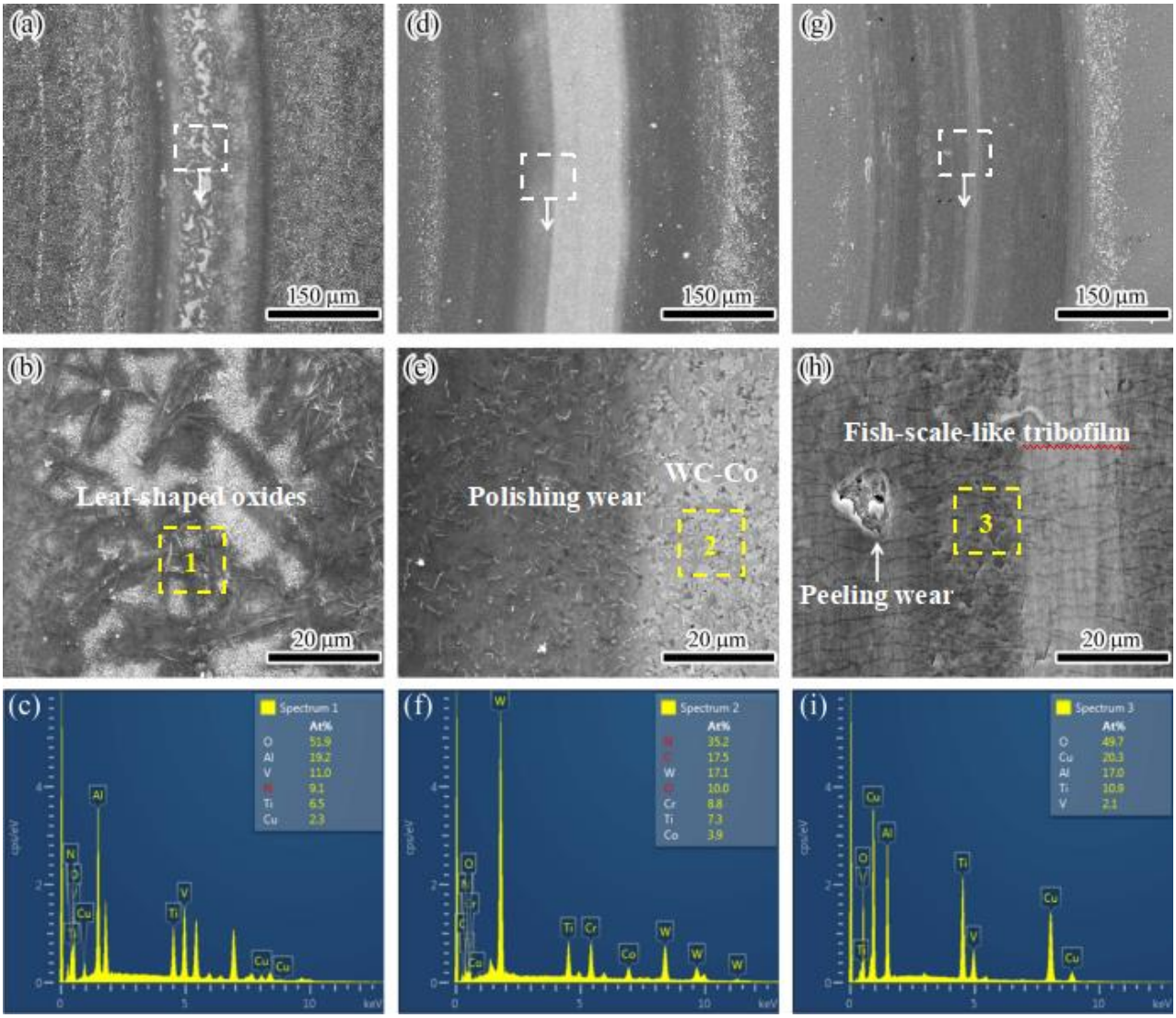

Fig. 10. Worn surfaces, high-magnification images and EDS results of the wear tracks at 600 °C: (a–c) $Al_{21}Ti_{12}V_{17}Cu_3N_{47}$, (d–f) $Al_{26}Ti_{14}V_9Cu_8N_{43}$, (g–i) $Al_{26}Ti_{14}V_3Cu_{22}N_{35}$.

area 1 revealed that these oxides were rich in elements Al, V and O, which corresponded to the $AlVO_4$ and V_2O_5 oxides based on above XRD results. Thus, it can be inferred that during the sliding process, the rod-shaped oxides on coating surface (in Fig. 6(a)) were compacted and sheared and formed leaf-shaped oxides on the worn surface in Fig. 10(b). Thus, the wear mechanism at 600 °C was dominated by severe oxidation wear, which led to a decrease in wear resistance. In Fig. 10(d–f), for the $Al_{26}Ti_{14}V_9Cu_8N_{43}$ coating, the wear track became increasingly wide, indicating that a decrease in wear resistance. The magnified image in Fig. 10(e) shows a polished worn surface, and the center area of the worn surface was rich in W, C, and Co, thereby implying that the coating was completely worn out and that the wear mechanism was dominated by polishing wear that was similar to that at RT. For the $Al_{26}Ti_{14}V_3Cu_{22}N_{35}$ coating in Fig. 10(g–i), the worn surface was relatively smooth and shallow, which indicated excellent wear resistance. In Fig. 10(h), the worn surface exhibited a smooth fish-scale-like tribofilm, and the EDS results revealed that the tribofilm was rich in elements Cu and O, which corresponded to the CuO based on the above XRD results, leading to a low friction coefficient (in Fig. 1(c)). The peeling off of oxidized particles (in Fig. 6(g)) also caused peeling wear during the sliding process, which implied that oxidation and peeling wear occurred in the coating.

To investigate the high-temperature tribo-oxidation behavior of Al-Ti-V-Cu-N coatings, XPS analysis was performed to identify the tribo-oxides on worn surfaces at 600 °C. Fig. 11 presents the fitted Al 2p, Ti 2p, V $2p_{3/2}$, and Cu $2p_{3/2}$ XPS spectra of the worn surfaces. As shown in Fig. 11(a), for the $Al_{21}Ti_{12}V_{17}Cu_3N_{47}$ coating, two peaks at 75.0 and 69.6 eV in the

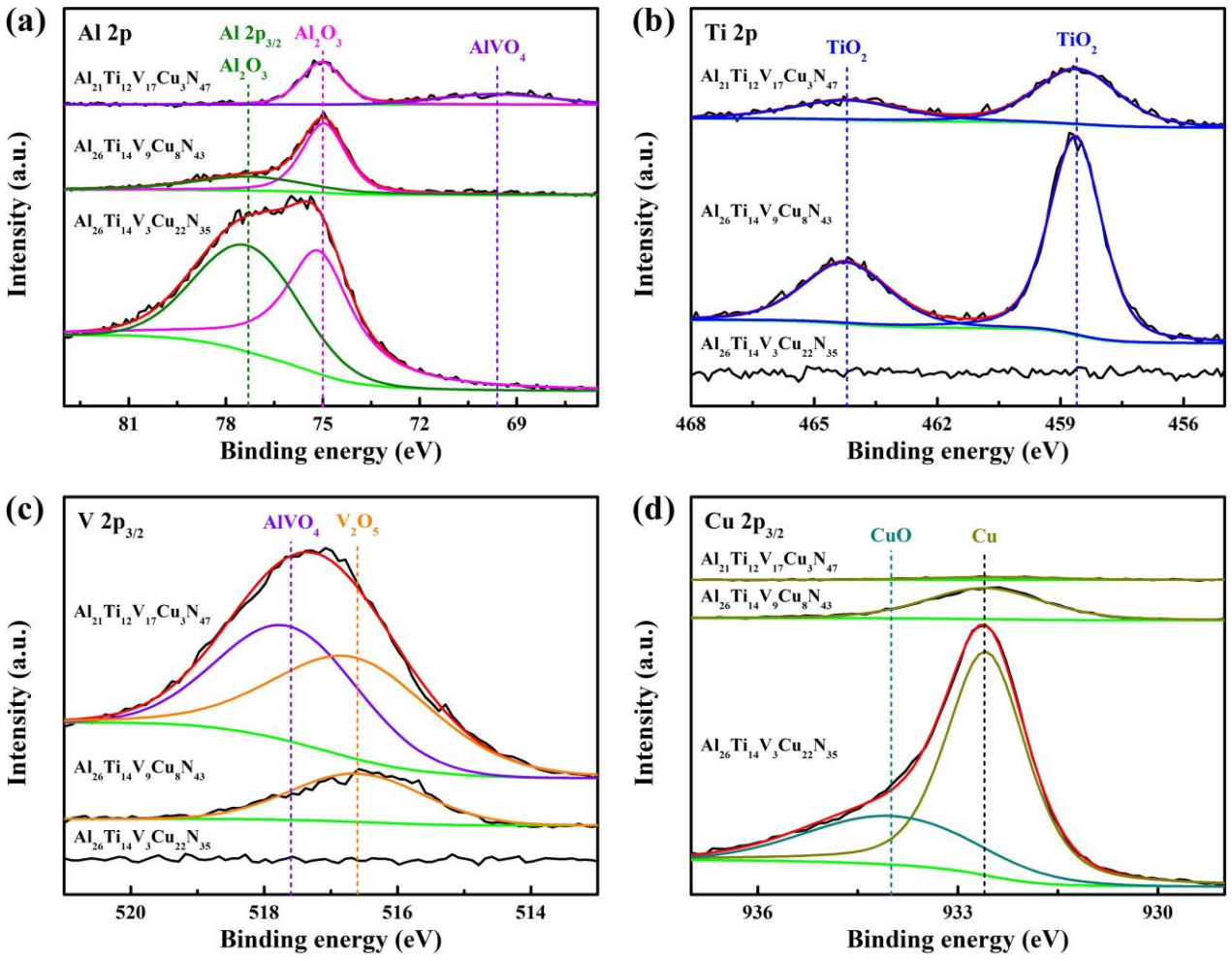

Fig. 11. Fitted XPS spectra of the worn surfaces after wear at 600 °C: (a) Al 2p, (b) Ti 2p, (c) V $2p_{3/2}$, and (d) Cu $2p_{3/2}$.

fitted Al 2p spectra were attributed to the Al_2O_3 and $AlVO_4$ oxides, respectively [28, 29]. However, when the V content decreased, for the $Al_{26}Ti_{14}V_9Cu_8N_{43}$ and $Al_{26}Ti_{14}V_3Cu_{22}N_{35}$ coatings, the $AlVO_4$ peak disappeared and was replaced by an Al_2O_3 peak at 77.3 eV in the Al $2p_{3/2}$ spectra. In Fig. 11(b), the asymmetric Ti 2p spectra consisted of two peaks at 458.6 and 464.2 eV, which corresponded to the TiO_2 species [30]. It has been found that the TiO_2 oxide with porous structure deteriorated the Al_2O_3 protective layer, thereby leading to a decrease in wear resistance [31]. However, for the $Al_{26}Ti_{14}V_3Cu_{22}N_{35}$ coating, the TiO_2 peak disappeared completely. In Fig. 11(c), for the $Al_{21}Ti_{12}V_{17}Cu_3N_{47}$ coating, two peaks at 516.6 and 517.6 eV in the V $2p_{3/2}$ spectrum were assigned to the V_2O_5 and $AlVO_4$, respectively [32, 33]. However, when the V content decreased, only the V_2O_5 peak was observed for the $Al_{26}Ti_{14}V_9Cu_8N_{43}$ coating, and the V_2O_5 peak also disappeared for the $Al_{26}Ti_{14}V_3Cu_{22}N_{35}$ coating. In Fig. 11(d), one peak centered at 932.6 eV in the Cu $2p_{3/2}$ spectra was assigned to metallic copper Cu [14], and the fraction of the Cu peak increased as the Cu content increased. For the $Al_{26}Ti_{14}V_3Cu_{22}N_{35}$ coating, a peak with a high binding energy of 934.0 eV corresponded to CuO, which was consistent with the above oxidation behavior at 600 °C. Thus, for the $Al_{21}Ti_{12}V_{17}Cu_3N_{47}$ coating, the worn surface was completely oxidized, and the oxides that formed on the worn surface were dominated by $AlVO_4$, V_2O_5, Al_2O_3, and TiO_2, which was related to the rapid oxidation and diffusion of Al-Ti-V-Cu-N coating at high temperatures. For the $Al_{26}Ti_{14}V_9Cu_8N_{43}$ coating, $AlVO_4$ oxide disappeared and formed the major oxide TiO_2. However, for the $Al_{26}Ti_{14}V_3Cu_{22}N_{35}$ coating, both V_2O_5 and TiO_2 disappeared and formed the major oxides CuO and Al_2O_3, which led to excellent wear resistance at 600 °C. This demonstrated that the major oxides that formed on the worn surface could directly affect the tribological behavior at elevated temperatures.

4. Conclusions

In this work, the co-doping of V and Cu exhibited a significant influence on the tribological properties and oxidation behavior of AlTiN coatings, and the diffusion- oxidation mechanisms of the coatings at elevated temperatures were explored in detail. As the Cu content increased and V content decreased, the wear rates of Al-Ti-V-Cu-N coatings at RT and 300 °C both increased from 10^{-15} to 10^{-14} $m^3/N{\cdot}m$. At 300 °C, as the Cu content increased to 22.6 at.%, Cu preferentially diffused outward through the voids around growth defects and formed a smooth surface, thereby resulting in a low friction coefficient value of 0.49. At 600 °C, the $Al_{26}Ti_{14}V_3Cu_{22}N_{35}$ coating provided a sufficient amount of Cu to diffuse outward and form a smooth top layer of CuO oxide, which exhibited an excellent lubrication effect and wear resistance, with a low friction coefficient of 0.5 and wear rate of 3.2×10^{-15} $m^3/N{\cdot}m$.

Acknowledgments

This work was supported by the National Natural Science Foundation of China (51875109, 51672100), the Guangdong Basic and Applied Basic Research Foundation (2020A1515110016), the International Science and Technology Cooperation Project of Guangdong Province (2019A050510049), the Professorial and Doctoral Scientific Research Foundation of Huizhou University (2020JB010), Indigenous Innovation's Capability Development Program of Huizhou University (HZU202005), Innovative Research Team of Guangdong Province and Huizhou University (IRTHZU).

References

[1] H. Poláková, J. Musil, J. Vlček, J. Allaart, C. Mitterer, Structure-hardness relations in sputtered Ti-Al-V-N

films, Thin Solid Films 444 (2003) 189–198.
[2] A.M. Abd El-Rahman, Synthesis and annealing effects on the properties of nanostructured Ti-Al-V-N coatings deposited by plasma enhanced magnetron sputtering, Mater. Chem. Phys. 149–150 (2015) 179–187.
[3] M. Jaroš, J. Musil, R. Čerstvý, S. Haviar, Effect of energy on structure, microstructure and mechanical properties of hard Ti(Al,V)N_x films prepared by magnetron sputtering, Surf. Coat. Technol. 332 (2017) 190–197.
[4] M. Jaroš, J. Musil, R. Čerstvý, S. Haviar, Effect of energy on macrostress in Ti(Al,V)N films prepared by magnetron sputtering, Vacuum 158 (2018) 52–59.
[5] M. Jaroš, J. Musil, S. Haviar, Interrelationships among macrostress, micro- structure and mechanical behavior of sputtered hard Ti(Al,V)N films, Mater. Lett. 235 (2019) 92–96.
[6] M. Pfeiler, K. Kutschej, M. Penoy, C. Michotte, C. Mitterer, M. Kathrein, The influence of bias voltage on structure and mechanical/tribological properties of arc evaporated Ti-Al-V-N coatings, Surf. Coat. Technol. 202 (2007) 1050–1054.
[7] R. Franz, C. Mitterer, Vanadium containing self-adaptive low-friction hard coatings for high-temperature applications: A review, Surf. Coat. Technol. 228 (2013) 1–13.
[8] M. Pfeiler, K. Kutschej, M. Penoy, C. Michotte, C. Mitterer, M. Kathrein, The effect of increasing V content on structure, mechanical and tribological properties of arc evaporated Ti-Al-V-N coatings, Int. J. Refract. Met. H. 27 (2009) 502–506.
[9] K. Kutschej, P.H. Mayrhofer, M. Kathrein, P. Polcik, C. Mitterer, A new low- friction concept for $Ti_{1-x}Al_xN$ based coatings in high-temperature applications, Surf. Coat. Technol. 188–189 (2004) 358–363.
[10] K. Kutschej, P.H. Mayrhofer, M. Kathrein, P. Polcik, C. Mitterer, Influence of oxide phase formation on the tribological behaviour of Ti-Al-V-N coatings, Surf. Coat. Technol. 200 (2005) 1731–1737.
[11] Y.X. Xu, L. Chen, F. Pei, J.L. Yue, Y. Du, Thermal stability and oxidation resistance of V-alloyed TiAlN coatings, Ceram. Int. 44 (2018) 1705–1710.
[12] C.P. Mulligan, T.A. Blanchet, D. Gall, Control of lubricant transport by a CrN diffusion barrier layer during high-temperature sliding of a CrN-Ag composite coating, Surf. Coat. Technol. 205 (2010) 1350–1355.
[13] C.P. Mulligan, T.A. Blanchet, D. Gall, CrN-Ag nanocomposite coatings: High- temperature tribological response, Wear 269 (2010) 125–131.
[14] J.H. Shin, Q.M. Wang, K.H. Kim, Microstructural evolution and tribological behavior of Mo-Cu-N coatings as a function of Cu content, Mater. Chem. Phys. 130 (2011) 870–879.
[15] G.S. Fox-Rabinovich, K. Yamamoto, M.H. Aguirre, D.G. Cahill, S.C. Veldhuis, A. Biksa, G. Dosbaeva, L.S. Shuster, Multi-functional nano-multilayered AlTiN/ Cu PVD coating for machining of Inconel 718 superalloy, Surf. Coat. Technol. 204 (2010) 2465–2471.
[16] V. Ezirmik, E. Senel, K. Kazmanli, A. Erdemir, M. Ürgen, Effect of copper addition on the temperature dependent reciprocating wear behaviour of CrN coatings, Surf. Coat. Technol. 202 (2007) 866–870.
[17] H. Mei, Q. Luo, X. Huang, J.C. Ding, T.F. Zhang, Q. Wang, Influence of lubricious oxides formation on the tribological behavior of Mo-V-Cu-N coatings deposited by HIPIMS, Surf. Coat. Technol. 358 (2019) 947–957.
[18] S. Zhu, J. Cheng, Z. Qiao, J. Yang, High temperature solid-lubricating materials: A review, Tribol. Int. 133 (2019) 206–223.
[19] H. Mei, D. Geng, R. Wang, L. Cheng, J.C. Ding, Q. Luo, T.F. Zhang, Q. Wang, Effect of Cu doping on the microstructure and mechanical properties of AlTiVN -Cu nanocomposite coatings, Surf. Coat. Technol. 402 (2020) 126490.
[20] Z. Zhou, W.M. Rainforth, Q. Luo, P.Eh. Hovsepian, J.J. Ojeda, M.E. Romero- Gonzalez, Wear and friction of TiAlN/VN coatings against Al_2O_3 in air at room and elevated temperatures, Acta. Mater. 58 (2010) 2912–2925.
[21] D.B. Lewis, S. Creasey, Z. Zhou, J.J. Forsyth, A.P. Ehiasarian, P.Eh. Hovsepian, Q. Luo, W.M. Rainforth, W.-D. Münz, The effect of (Ti+Al):V ratio on the structure and oxidation behaviour of TiAlN/VN nano-scale multilayer coatings, Surf. Coat. Technol. 177–178 (2004) 252–259.
[22] W. Dai, S.H. Kwon, Q. Wang, J. Liu, Influence of frequency and C_2H_2 flow on growth properties of diamond-like carbon coatings with AlCrSi co-doping deposited using a reactive high power impulse magnetron sputtering, Thin Solid Films 647 (2018) 26–32.
[23] Z. Zhou, W.M. Rainforth, C. Rodenburg, N.C. Hyatt, D.B. Lewis, P.E. Hovsepian, Oxidation behavior and mechanisms of TiAlN/VN coatings, Metall. Mater. Trans. A 38 (2007) 2464–2478.
[24] M. Pfeiler, G.A. Fontalvo, J. Wagner, K. Kutschej, M. Penoy, C. Michotte, C. Mitterer, M. Kathrein, Arc evaporation of Ti-Al-Ta-N coatings: the effect of bias voltage and Ta on high-temperature tribological properties, Tribol. Lett. 30 (2008) 91–97.
[25] F. Vaz, L. Rebouta, M. Andritschky, M.F. Silva, J.C. Soares, Oxidation resistance of (Ti, Al, Si)N coatings in air, Surf. Coat. Technol. 98 (1998) 912– 917.
[26] B.D. Beake, J.F. Smith, A. Gray, G.S. Fox-Rabinovich, S.C. Veldhuis, J.L. Endrino, Investigating the correlation between nano-impact fracture resistance and hardness/modulus ratio from nanoindentation at

25–500 °C and the fracture resistance and lifetime of cutting tools with TiAlN PVD coatings in milling operations, Surf. Coat. Technol. 201 (2007) 4585–4593.
[27] Q. Luo, Temperature dependent friction and wear of magnetron sputtered coating TiAlN/VN, Wear 271 (2011) 2058–2066.
[28] T. Wang, G. Zhang, B. Jiang, Comparison in mechanical and tribological properties of CrTiAlMoN and CrTiAlN nano-multilayer coatings deposited by magnetron sputtering, Appl. Surf. Sci. 363 (2016) 217–224.
[29] J.R. Lindsay, H.J. Rose, W.E. Swartz, P.H. Watts, K.A. Rayburn, X-ray photoelectron spectra of aluminum oxides: structural effects on the “chemical shift”, Appl. Spectrosc. 27 (1973) 1–5.
[30] M.P. Deutschmann, P.H. Mayrhofer, K. Chladil, M. Penoy, C. Michotte, M. Kathrein, C. Mitterer, Effect of wavelength modulation of arc evaporated Ti-Al-N/Ti-Al-V-N multilayer coatings on microstructure and mechanical/ tribological properties, Thin Solid Films 581 (2015) 20–24.
[31] M. Pfeiler, J. Zechner, M. Penoy. C. Michotte, C. Mitterer, M. Kathrein, Improved oxidation resistance of TiAlN coatings by doping with Si or B, Surf. Coat. Technol. 203 (2009) 3104–3110.
[32] N.K. Nag, F.E. Massoth, ESCA and gravimetric reduction studies on V/Al_2O_3 and V/SiO_2 catalysts, J. Catal. 124 (1990) 127–132.
[33] Y. Chen, Z. Zhang, T. Yuan, F. Mei, X. Lin, J. Gao, W. Chen, Y. Xu, The synergy of V and Si on the microstructure, tribological and oxidation properties of AlCrN based coatings, Surf. Coat. Technol. 412 (2021) 127082.